Available online at www.sciencedirect.com
ScienceDirect
Mechanical Systems and Signal Processing 23 (2009) 148–169
Mechanical Systems and Signal Processing
www.elsevier.com/locate/jnlabr/ymssp

# Using passive nonlinear targeted energy transfer to stabilize drill-string systems

R. Viguié[a], G. Kerschen[a,*], J.-C. Golinval[a], D.M. McFarland[b], L.A. Bergman[b], A.F. Vakakis[c,d,e], N. van de Wouw[f]

[a]Aerospace and Mechanical Engineering Department (LTAS), University of Liège, 1 Chemin des Chevreuils, B-4000 Liège, Belgium
[b]Department of Aerospace Engineering, University of Illinois at Urbana-Champaign, USA
[c]Division of Mechanics, National Technical University of Athens, Greece
[d]Department of Mechanical Science and Engineering, University of Illinois at Urbana-Champaign, USA
[e]Department of Aerospace Engineering (adjunct), University of Illinois at Urbana-Champaign, USA
[f]Department of Mechanical Engineering, Group Dynamics and Control, Eindhoven University of Technology, The Netherlands

Received 27 March 2007; received in revised form 12 June 2007; accepted 5 July 2007
Available online 20 July 2007

**Abstract**

Torsional vibrations of drill strings used in drilling oil and gas wells arise from a complex interaction of the dynamics of the drilling structure with speed-dependent effective rock-cutting forces. These forces are often difficult to model, and contribute substantially to the instability problems of controlling the drilling operation so as to produce steady cutting. In this work we show how nonlinear passive targeted energy transfer to a lightweight attachment can be used to passively control these instabilities. This is performed by means of a nonlinear energy sink (NES), a lightweight attachment which has been shown to be effective in reducing or even completely eliminating self-excited motions in aeroelastic and other systems. The NES is a completely passive, inherently broadband vibration absorber capable of attracting and dissipating vibrational energy from the primary structure to which it is attached, in this case a nonlinear discontinuous model of a drill-string system. In this paper we describe a prototypical drill string-NES system, briefly discuss some of the analytical and computational tools suitable for its analysis, and then concentrate on mathematical results on the efficacy of the NES in this application and their physical interpretation.


*Keywords:* Drill-string system; Torsional vibrations; Passive energy transfer; Essential nonlinearity; Nonlinear energy sink

## 1. Introduction

In drilling deep oil and gas wells, it can be difficult to maintain smooth cutting at the bit-rock interface. Among other disturbances, the rock is not homogeneous, the unavoidable friction is complicated by fluid flow,

*Corresponding author. Tel.: +32 4 3669098; fax: +32 4 3664856.
*E-mail addresses:* r.viguie@ulg.ac.be (R. Viguié), g.kerschen@ulg.ac.be (G. Kerschen), jc.golinval@ulg.ac.be (J.-C. Golinval), dmmcf@uiuc.edu (D.M. McFarland), lbergman@uiuc.edu (L.A. Bergman), vakakis@central.ntua.gr, avakakis@uiuc.edu (A.F. Vakakis), N.v.d.Wouw@tue.nl (N. van de Wouw).

0888-3270/$ - see front matter 
doi:10.1016/j.ymssp.2007.07.001

and spatially asymmetric, time-varying forces may be introduced to "steer" the well bore. All of these effects interact with the drill string, which itself can be several thousand meters long, to produce a dynamic environment which can exhibit inadequate stability.

In this paper we address the problem of stabilizing the dynamics of the drill-string system by means of nonlinear passive targeted energy transfer, i.e., by adding a passive, spatially localized attachment; a nonlinear energy sink (NES). The phenomenon we seek to exploit is that of targeted energy transfer, or *nonlinear energy pumping*, which has been studied in a number of recent papers (see, e.g., [1–3]). The NES here takes the form of a discrete torsional oscillator comprising a disk coupled to the drill string system through an essentially nonlinear spring and a viscous damper. Mathematically, similar devices of various configurations have been shown to be effective in suppressing transient responses to broadband external loads and in reducing or eliminating self-excited vibrations in a van der Pol oscillator and in aeroelastic systems [4,5]. The present use bears some similarities to the latter class of applications, but differs qualitatively in the large spatial separation between the driving motor and the drill bit.

Following a precise statement of the problem to be studied, we review some of the numerical challenges in analyzing a drill-string system model. Most of these are found to arise from the need to efficiently compute dynamic responses in the presence of friction and related discontinuities. A bifurcation diagram depicting the behavior of the system over a realistic range of inputs is produced, and is used to assess the influence of the NES parameters on the dynamics of the integrated system. A numerical study and the resulting NES design is described next. Finally, a detailed analysis of the integrated system composed of a drill string system and attached NES is presented, including some remarks on the robustness of the passive control achieved with this device.

## 2. Problem description

Deep wells for the exploration and production of oil and gas are drilled with a rotary drilling system (Fig. 1). A rotary drilling system creates a borehole by means of a rock-cutting tool, called the bit. The torque driving the bit is generated at the surface by a motor with a mechanical transmission box. Via the transmission, the motor drives the rotary table that consists in a large disk acting as a kinetic energy storage unit. The medium to transport the energy from the surface to the bit is a drill-string, mainly consisting of drill pipes. The drill-string can be up to 8 km long. The lowest part of the drill-string is the bottom-hole-assembly

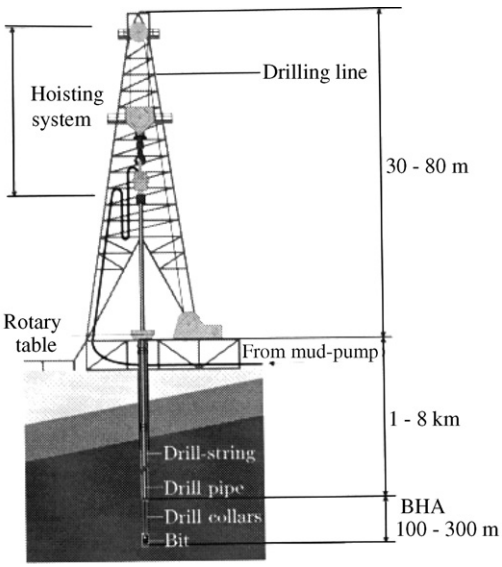


Fig. 1. Schematic view of the structure [6].

(BHA) consisting of drill collars and the bit. This structure undergoes different kinds of vibrations during the drilling operation, including:

(1) *Torsional* (*rotational*) *vibrations* caused by the interaction between the bit and the rock or the drill-string and the borehole wall.
(2) *Bending* (*lateral*) *vibrations* often caused by pipe eccentricity leading to centripetal forces during rotation.
(3) *Axial* (*longitudinal*) *vibrations* due to rock cutting process (an extreme form is called bit bouncing).
(4) *Hydraulic vibrations* taking place in the circulation system, coming from pump pulsations.

In addition, there exist coupling effects between torsional, lateral and longitudinal vibrations, as highlighted in [6,7]. In this paper, our efforts are devoted to vibration mitigation of torsional vibrations. Many studies were undertaken to gain improved knowledge of the origins of those vibrations [8–13]. It was established that a possible mechanism for torsional vibration is the stick-slip phenomenon generated by the friction force between the bit and the well [9–11]. Other studies [12,13] showed that the cause of torsional vibrations is velocity weakening in the friction force (i.e., Stribeck effect) due to the contact between the bit and the borehole. In [14,15], it is shown that such velocity weakening effect originates from a coupling between the torsional and axial dynamics through the bit/rock interaction. Ultimately, this velocity weakening effect plays a very important role in the occurrence of limit cycling in drill-string systems [16].

To examine this instability, a prototypical drill-string system was built at the Technische Universiteit Eindhoven [6,16]. Fig. 2 depicts the experimental set-up, whereas Fig. 3 shows its schematic representation. The system comprises two discs that model the inertia effects created by the rotating components in the upper (e.g., rotary table) and lower (e.g., BHA) parts. For further details about the experimental fixture, the interested reader may refer to [6,16].

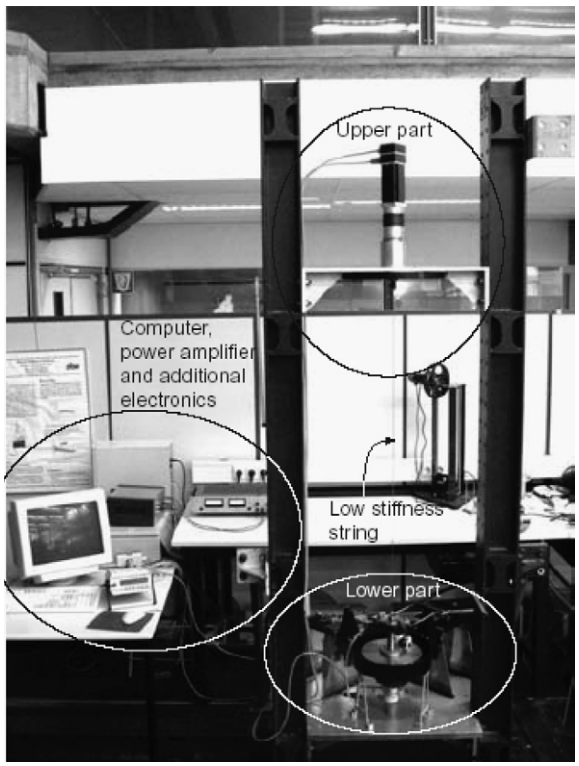


Fig. 2. Experimental drill-string set-up [6,16].

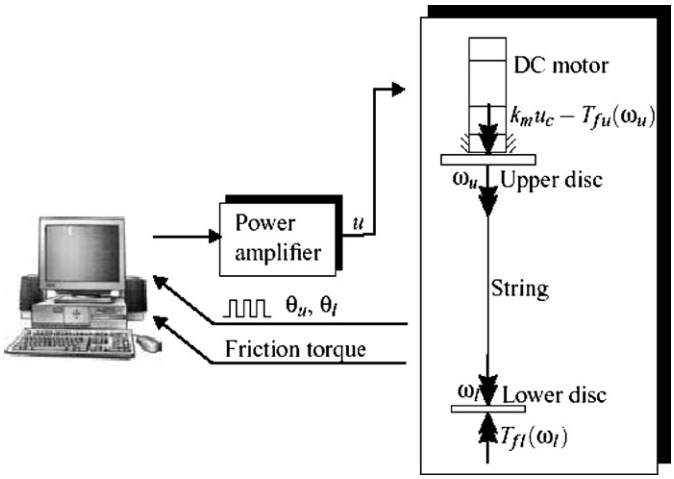


Fig. 3. Schematic view of the set-up [6,16].

Table 1
Definitions

| | |
|---|---|
| $\omega_u\ (=\dot{\theta}_u)$ | Velocity of the upper disc |
| $\omega_l\ (=\dot{\theta}_l)$ | Velocity of the lower disc |
| $J_u, J_l$ | Moment of inertia of the upper and lower disc about their respective centers |
| $k_m$ | Motor constant |
| $T_{fu}, T_{fl}$ | Friction torque at the upper and lower disc |
| $k_\theta$ | Torsional spring stiffness |
| $\theta_u, \theta_l$ | Angular displacements of the upper and lower disc |
| $\alpha = \theta_l - \theta_u$ | Relative angular displacement |
| $u_c$ | Input voltage at the DC-motor |

Because the focus of this paper is on torsional vibration, lateral movements of the system are restrained. This results in a reduced order two-degree-of-freedom model, the equations of motion of which are given by

$$\begin{cases} J_u\dot{\omega}_u - k_\theta\alpha + T_{fu}(\omega_u) = k_m u_c, \\ J_l(\ddot{\alpha} + \dot{\omega}_u) + T_{fl}(\omega_u + \dot{\alpha}) + k_\theta\alpha = 0. \end{cases} \tag{1}$$

The definition of the parameters in these equations is given in Table 1.

For modeling friction in the set-up, either static or dynamic friction models can be considered. Because the main objective of the present study is the analysis of the steady-state behavior of the drill-string system, a detailed dynamic modeling of friction for small angular velocities is not necessary. Therefore, a static friction model is adopted here.

Both discs are subject to friction torques ($T_f$) resulting from the action of different sources:

- At the upper disc, the friction torque $T_{fu}$ is due to friction in the bearings, as well as electro-magnetic effects in the DC-motor.
- At the lower disc, the friction torque $T_{fl}$ is due to friction in the bearings, as well as due to a brake mechanism that aims to reproduce the Stribeck effect.

It follows that both discs are subject to a torque which results from the combination of static ($T_s$) and viscous friction (through a viscous friction coefficient $b$). Moreover, at the lower disc, the presence of the Stribeck effect imposes the combination of the previous contributions in a Stribeck model. This model introduces new parameters such as, the Stribeck velocity ($\omega_{sl}$), the Stribeck shape parameter ($\delta_{sl}$) and the Coulomb friction

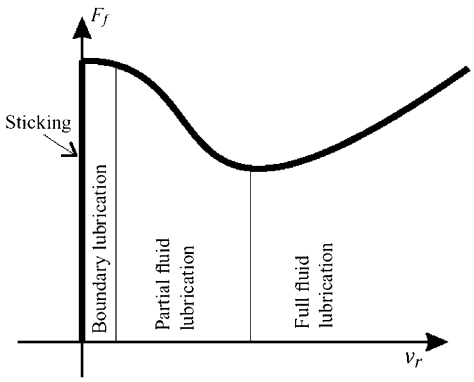


Fig. 4. Different regimes in the friction force, $F_f$ is the friction force and $v_r$ the relative velocity.

coefficient ($T_c$). The resulting curve corresponding to the friction force is depicted in Fig. 4 and can be divided into four different regimes: sticking, boundary lubrication, partial fluid lubrication and full fluid lubrication. All of these regimes as well as further details about this model can be found in [6,17–21]. Summarizing, the friction torques acting on each disc can be expressed by the following set-valued force laws:

$$T_{fu}(\omega_u) \in \begin{cases} T_{cu}(\omega_u)\,\mathrm{sgn}(\omega_u) & \text{for } \omega_u \neq 0, \\ [-T_{su}, T_{su}] & \text{for } \omega_u = 0, \end{cases} \tag{2}$$

$$T_{fl}(\omega_l) \in \begin{cases} T_{cl}(\omega_l)\,\mathrm{sgn}(\omega_l) & \text{for } \omega_l \neq 0, \\ [-T_{cl}(0^-), T_{cl}(0^+)] & \text{for } \omega_l = 0, \end{cases} \tag{3}$$

where subscripts '$u$' and '$l$' refer to upper and lower parts of the set-up, respectively; $T_{cu}(\omega_u)$ and $T_{cl}(\omega_l)$ express the velocity dependency of the friction at the upper and lower discs, respectively. In the above expressions, the terms $T_{cu}(\omega_u)$ and $T_{cl}(\omega_l)$ are defined as follows:

$$T_{cu}(\omega_u) = T_{su} + b_u|\omega_u|, \tag{4}$$

$$T_{cl}(\omega_l) = T_{cbl} + (T_{sl} - T_{cbl})e^{-|\omega_l/\omega_{sl}|^{\delta_{sl}}} + b_l|\omega_l|, \tag{5}$$

where $T_{sl}$ and $T_{cbl}$ refer, respectively, to the static friction and Coulomb friction torque at the lower disc. Figs. 5 and 6 depict the dependency of both torques with the related angular velocity of their related disc.

Although the present study focuses on numerical experiments using the two-degree-of-freedom model (1), the same parameters as those identified for the experimental set-up in Ref. [6] are adopted. These are listed in Table 2.

## 3. Instability of the two-degree-of-freedom drill string model

The objective of this section is to study the steady-state behavior of the reduced two-DOF drill-string model. The steady-state behavior for constant input voltage $u_c$ is of particular interest since these types of systems are generally driven by a constant torque while aiming at a constant velocity at the lower part of the set-up. The presence of friction and related discontinuities in the equations of motion requires the use of appropriate numerical algorithms to efficiently compute the dynamic responses.

### 3.1. Numerical integration using the switch model

A $n$th-order autonomous nonlinear dynamical system is defined by the following differential equation:

$$\dot{\mathbf{x}} = \mathbf{f}(\mathbf{x}), \tag{6}$$

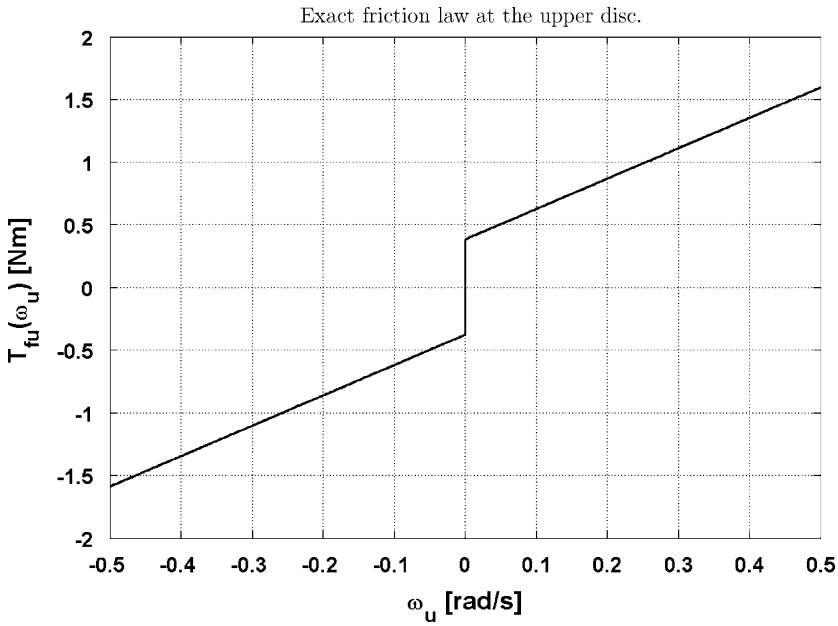


Fig. 5. Friction model at the upper disc.

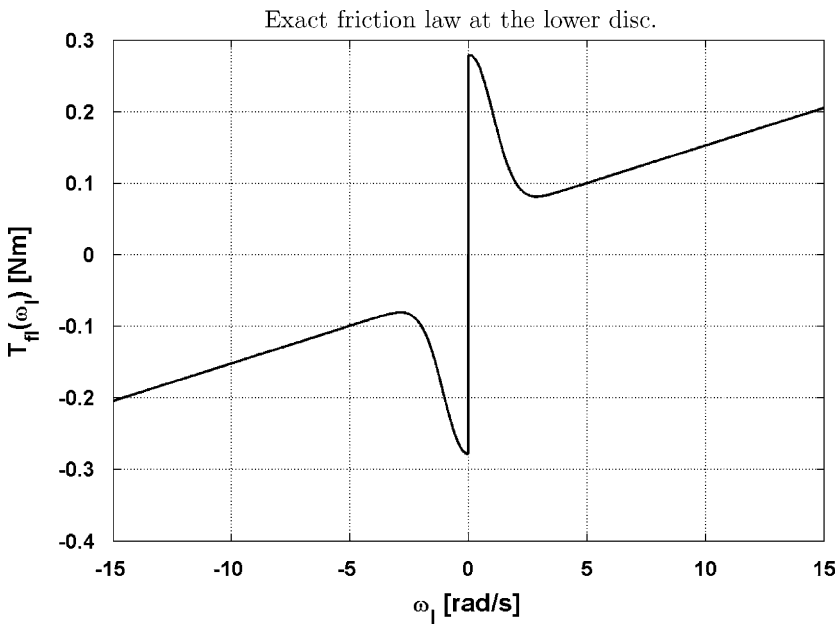


Fig. 6. Friction model at the lower disc.

with initial condition

$$\mathbf{x}(t_0) = \mathbf{x}_0, \tag{7}$$

where $\mathbf{x} \in \mathbb{R}^n$ represents the state vector, $t \in \mathbb{R}$ represents the time, and $\mathbf{f}$: $\mathbb{R}^n \to \mathbb{R}^n$ is called a *vector field*.

Table 2
Parameters of the two-degree-of-freedom drill-string system

| Parameter | Units | Estimated value |
|---|---|---|
| $J_u$ | (kg m$^2$/rad) | 0.4765 |
| $k_m$ | (N m/V) | 4.3228 |
| $T_{su}$ | (N m) | 0.37975 |
| $b_u$ | (N m s/rad) | 2.4245 |
| $k_\theta$ | (N m/rad) | 0.0775 |
| $J_l$ | (kg m$^2$/rad) | 0.0414 |
| $T_{sl}$ | (N m) | 0.2781 |
| $T_{cl}$ | (N m) | 0.0473 |
| $\omega_{sl}$ | (rad/s) | 1.4302 |
| $\delta_{sl}$ | (–) | 2.0575 |
| $b_l$ | (N m s/rad) | 0.0105 |

The discontinuous characteristics of the friction laws acting on the system imply that the vector field $\mathbf{f}$ in Eq. (6) is also discontinuous. Therefore, the right-hand side of this equation can be written as

$$\dot{\mathbf{x}} = \mathbf{f}(\mathbf{x}) = \begin{cases} \mathbf{f}_-(\mathbf{x}) & \text{for } \mathbf{x} \in \Lambda_-, \\ \mathbf{f}_+(\mathbf{x}) & \text{for } \mathbf{x} \in \Lambda_+, \end{cases} \tag{8}$$

when considering a single discontinuity. The vector field $\mathbf{f}$ is assumed to be piecewise continuous and smooth on $\Lambda_-$ and $\Lambda_+$ and discontinuous on a hyper-surface $\Sigma$ with

$$\begin{aligned} \Sigma &= \{\mathbf{x} \in \mathbb{R}^n | g(\mathbf{x}) = 0\}, \\ \Lambda_- &= \{\mathbf{x} \in \mathbb{R}^n | g(\mathbf{x}) < 0\}, \\ \Lambda_+ &= \{\mathbf{x} \in \mathbb{R}^n | g(\mathbf{x}) > 0\}, \end{aligned} \tag{9}$$

where the smooth mapping $g$: $\mathbb{R}^n \to \mathbb{R}$ defines the switching surface $\Sigma$. The system described by Eq. (8) is not defined if $\mathbf{x}$ is on $\Sigma$. We can overcome this limitation by introducing the following set-valued extension $\mathbf{F}(\mathbf{x})$ (of $\mathbf{f}(\mathbf{x})$):

$$\dot{\mathbf{x}} \in \mathbf{F}(\mathbf{x}) = \begin{cases} \mathbf{f}_-(\mathbf{x}) & \text{for } \mathbf{x} \in \Lambda_-, \\ [\mathbf{f}_-(\mathbf{x}), \mathbf{f}_+(\mathbf{x})] & \text{for } \mathbf{x} \in \Sigma, \\ \mathbf{f}_+(\mathbf{x}) & \text{for } \mathbf{x} \in \Lambda_+, \end{cases} \tag{10}$$

with

$$[\mathbf{f}_-(\mathbf{x}), \mathbf{f}_+(\mathbf{x})] = \{(1-q)\mathbf{f}_-(\mathbf{x}) + q\mathbf{f}_+(\mathbf{x}) \ \forall q \in [0,1]\}.$$

The extension (10) of the discontinuous system (8) is called a *differential inclusion* (note that in our case, the differential inclusion consists of the set of Eqs. (1)–(5)). This concept is important as it forms the basis of the numerical technique that is described in what follows.

The so-called *switch model* aims in approximating a differential inclusion by sets of ordinary differential equations. This concept is explained in great details in [22], and the main results are considered below. In order to numerically integrate the differential inclusion (10), the switch model introduces a boundary layer with thickness $2\eta$ around the hypersurface $\Sigma$ defined in (9). Within the boundary layer, a vector field is introduced such that the state of the system is pushed towards $\Sigma$ if an attractive sliding mode appears, avoiding numerical problems such as chattering of the solution around the sliding mode. Note that the term *sliding mode* means that once on the hypersurface $\Sigma$, the solution will not leave it and will go on moving on this switching

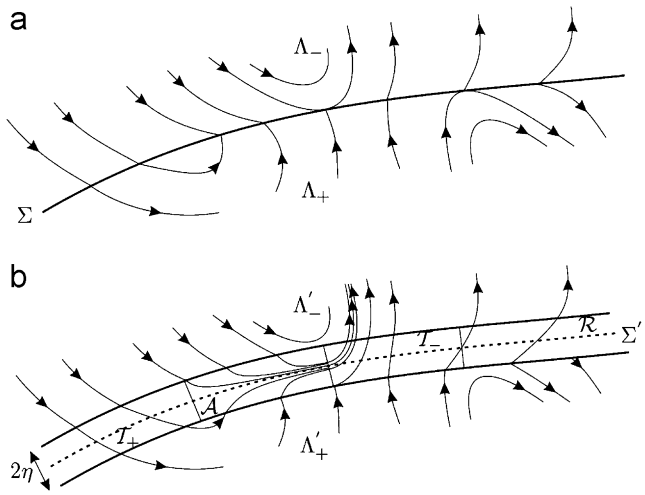


Fig. 7. Numerical approximation of a sliding mode using the switch model [6].

boundary. The state space $\mathbb{R}^n$ is divided into the following subspaces (see Fig. 7):

$$\begin{aligned}
\Sigma' &= \{\mathbf{x} \in \mathbb{R}^n \,|\, |g(\mathbf{x})| \leqslant \eta\},\\
\Lambda'_- &= \{\mathbf{x} \in \mathbb{R}^n | g(\mathbf{x}) < -\eta\},\\
\Lambda'_+ &= \{\mathbf{x} \in \mathbb{R}^n | g(\mathbf{x}) > \eta\}.
\end{aligned} \tag{11}$$

Then the subspace $\Sigma'$ is divided into subspaces $\mathscr{A}$, $\mathscr{R}$, $\mathscr{T}_-$ and $\mathscr{T}_+$ of vector fields $\mathbf{f}_+(\mathbf{x})$ and $\mathbf{f}_-(\mathbf{x})$ with respect to $\Sigma$. Each of these new subspaces has a particular feature: $\mathscr{A}$ contains an attractive sliding mode; $\mathscr{R}$ contains repulsive sliding mode; $\mathscr{T}_-$ and $\mathscr{T}_+$ are such that the solution has a transversal intersection from $\Lambda'_+$ to $\Lambda'_-$ and $\Lambda'_-$ to $\Lambda'_+$, respectively. For each of these subspaces, an appropriate approximation of the differential inclusion (10) can be formulated.

The main disadvantage of this model is the rapidly increasing complexity of the logical structure with increasing number of switching boundaries. Therefore, for such systems, more sophisticated simulation methods can be used as event-driven integration and time-stepping methods. For any further details about these concepts and methods, as well as a full description of the related algorithms, the reader can refer to [22].

### 3.2. Bifurcation diagrams

The numerical integration process may reveal the presence of steady-state solutions such as equilibrium points and periodic solutions. Here, we construct such a bifurcation diagram for the parameter settings as in Table 2 (see [6,16] for extensive bifurcation analyses for the drill-string model under study). In order to obtain accurate approximations of these solutions and their related stability, specific numerical methods and stability analysis techniques have to be considered:

- Stable equilibrium points can be easily computed using numerical simulations, but a more general method consists of the resolution of the algebraic inclusion of the discontinuous system. Moreover, the related stability (local and global) can be determined using Lyapunov's indirect and direct methods.
- For the computation of stable and unstable periodic solutions, the shooting method is used in this study [23]. This method relies on an iterative process and requires an initial guess. The local stability of the periodic solutions is determined using Floquet theory.
- The association of the previous methods with the arclength continuation method enables us to compute the bifurcation diagram of the system. The constant input voltage is chosen as the bifurcation parameter.

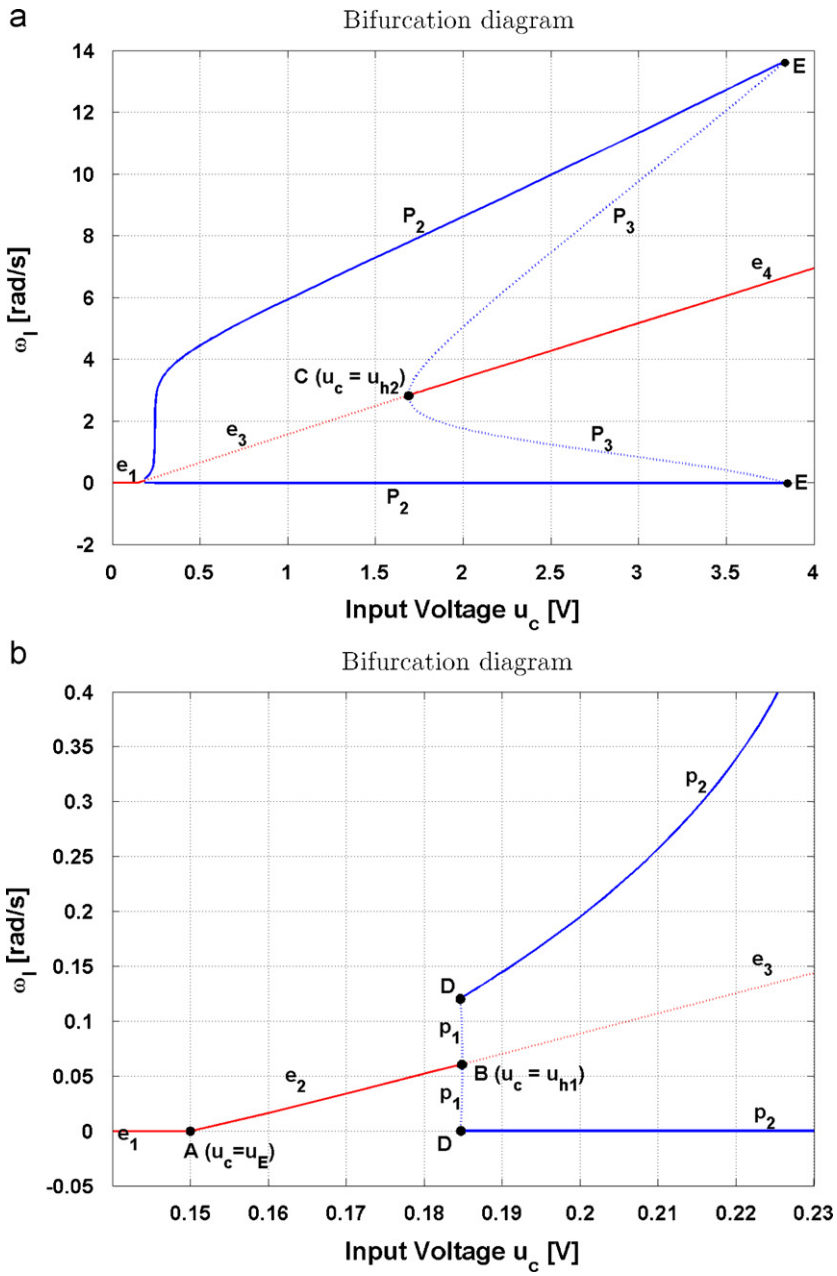


Fig. 8. Bifurcation diagram of the two-degree-of-freedom drill-string system: (a) bifurcation diagram; and (b) close-up of the low voltage range.

Throughout this study, we adopt an identical terminology for the bifurcation diagrams. The periodic solutions, that lead to limit cycle oscillations (LCOs), and the branches of equilibrium positions are denoted by '*p*' and '*e*', respectively. Solid and dotted lines refer to stable and unstable branches, respectively. The bifurcation diagram corresponding to system (1)–(5) for parameters listed in Table 2 is depicted in Fig. 8(a). The following description can be made regarding branches of equilibrium points:

- $u_c \leqslant u_E$: Locally asymptotically stable equilibrium set that gives the equilibrium branch $e_1$.
- $u_E \leqslant u_c \leqslant u_{h1}$: Locally asymptotically stable equilibrium points that constitute the equilibrium branch $e_2$.

- $u_{h1} \leqslant u_c \leqslant u_{h2}$: Unstable equilibrium points that constitute the equilibrium branch $e_3$.
- $u_{h2} \leqslant u_c$: Both locally and globally asymptotically stable equilibrium points (depending on the value $u_c$) that gives the equilibrium branch $e_4$.

LCOs are generated due to a steady-state balance between the 'stabilizing' effect of viscous friction (at higher velocities) and the 'destabilizing' effect of the Stribeck effect (at lower velocities) (see [16]). We note that:

- From point B, in addition to the unstable equilibrium branch $e_3$, we have a periodic branch $p_1$ that consists of unstable limit cycles without stick-slip. B is a subcritical Hopf bifurcation point.

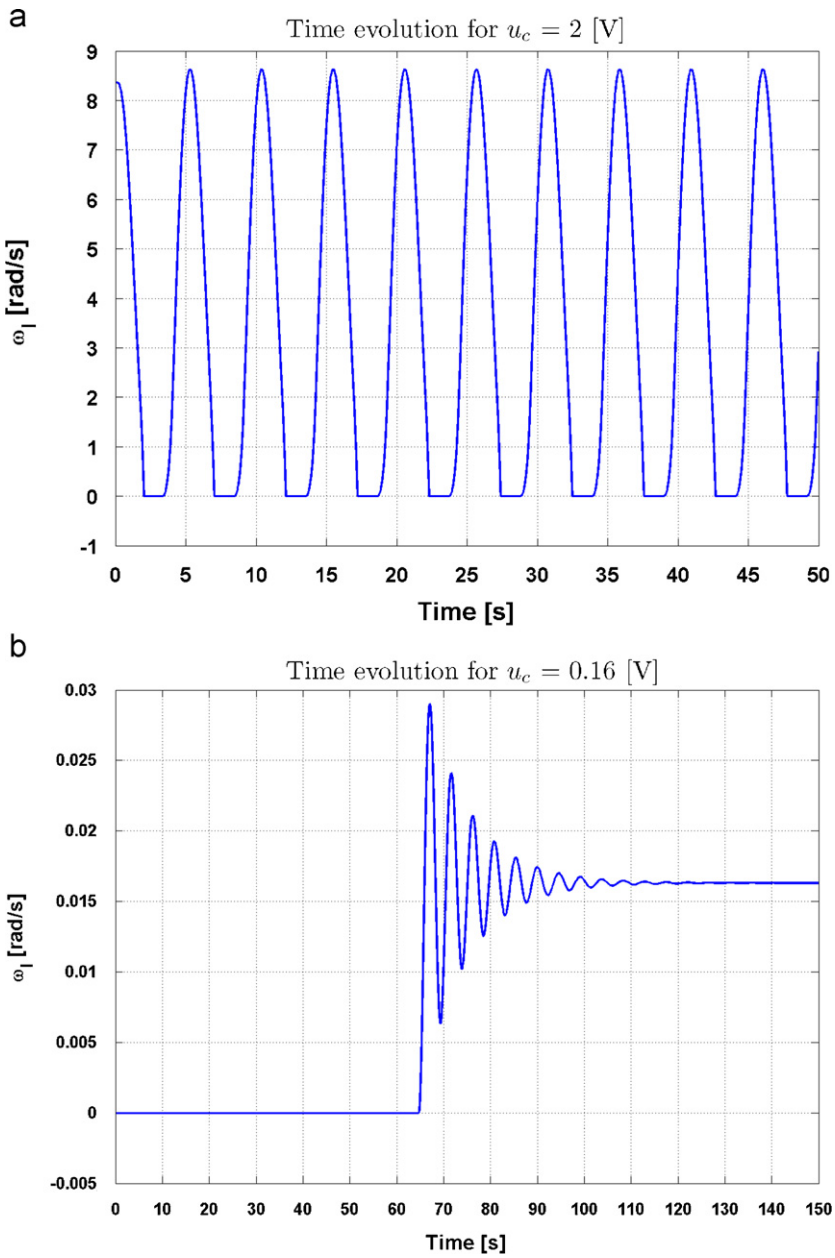


Fig. 9. (a) LCO with stick-slip phenomenon ($u_c = 2$ V); and (b) transition to an equilibrium point ($u_c = 0.16$ V).

- The periodic branch $p_1$ is connected to the locally stable periodic branch $p_2$ at point D. Because $p_2$ consists of LCOs (torsional vibration) with stick-slip, D is a discontinuous fold bifurcation.
- At point E, the locally stable limit cycles merge with an unstable branch $p_3$ of periodic solutions. E is a discontinuous fold bifurcation point.
- Branch $p_3$ is connected to equilibrium branches $e_3$ and $e_4$ at the subcritical Hopf bifurcation point C.

For illustration, the time series corresponding to LCO motion and attraction toward an equilibrium point are given in Fig. 9.

## 4. Suppression of friction-induced limit cycles by means of a NES: a parametric study

For vibration mitigation in mechanical systems, active or passive methods can be used. In this study, a completely passive, inherently broadband vibration absorber is considered. One advantage is that it brings only relatively minor structural modifications to the primary structure. Moreover, it does not need any external energy supply to work.

### *4.1. Addition of the NES to the drill-string system*

The tuned mass damper (TMD) is a simple and efficient device, but it is only effective when it is precisely tuned to the frequency of a vibration mode. In our case, the nonlinear primary system presents the same vibration mode but the LCOs have a frequency that varies with the input voltage $u_c$. In this case, the TMD would be tuned on a particular frequency of the LCOs of the primary system, a feature which clearly limits its efficiency. To overcome the limitations of the TMD, an essentially nonlinear attachment (i.e., characterized by the absence of a linear term in the force-displacement relation), termed a NES, has been introduced. As shown in [2,3], an NES is characterized by two remarkable properties:

(1) The NES has no preferential resonant frequency, which enables it to engage in resonance with any mode of the system, irrespective of the frequency range. For instance, it may virtually resonate with and extract energy from any mode of a primary structure through resonance captures. By the term resonance capture we mean resonance between the dynamics of the NES and a mode of the system, which occurs, however, over a finite time range, and is followed by 'escape' from resonance capture when the instantaneous frequency of the NES escapes from the neighborhood of the eigenfrequency of that mode. Note that in our case, the power of the NES lies in dealing with the varying frequency of the stick-slip LCOs.
(2) Targeted energy transfer (i.e., an irreversible energy flow) from a primary structure to an attached NES can be achieved through either single resonance captures, or resonance capture cascades (e.g., resonance captures of the dynamics of the NES with a series of modes of the system to which it is attached). Hence, broadband targeted energy transfer from the system to the NES may occur.

The use of an NES therefore seems promising for vibration mitigation of nonlinear primary systems such as a drill-string system, since passive targeted energy transfers from the system to the NES can reduce the amplitude of vibration, or even completely eliminate instabilities. However, the increased complexity of the dynamical behaviour of a system with an attached NES is to be carefully studied, because of the strongly nonlinear characteristic of this attachment.

The addition of the NES results in an additional degree-of-freedom, a disc with moment of inertia $J_{\mathrm{add}}$, linked to the lower disc of the initial system through the combination of a cubic stiffness, $k_{\theta_{nl}}$ and a dashpot with damping coefficient $c_a$ (Fig. 10). The only degree of freedom of this disc is the rotation around its geometric center $\theta_a$, whereas any lateral motion is prohibited. The equations of motions of the system with

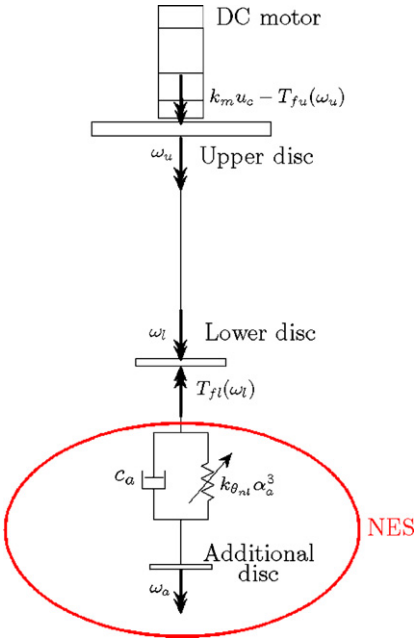


Fig. 10. Schematic representation of the drill-string system with an NES.

Table 3
Initial set of parameters

| Parameter | Units | Initial value |
|---|---|---|
| $J_{\text{add}}$ | (kg m$^2$/rad) | 0.025895 |
| $c_a$ | (N m s/rad) | 0.0105 |
| $k_{\theta_{nl}}$ | (N m/rad$^3$) | 0.0025 |

NES attached are

$$\begin{cases} J_u(\dot{\omega}_l - \ddot{\alpha}) - k_\theta \alpha + T_{fu}(\dot{\alpha} + \omega_l) = k_m u, \\ J_l(\dot{\omega}_l) + k_\theta \alpha - k_{\theta_{nl}}(\alpha_a)^3 - c_a \dot{\alpha}_a + T_{fl}(\omega_l) = 0, \\ J_{\text{add}}(\ddot{\alpha}_a + \dot{\omega}_l) + k_{\theta_{nl}}(\alpha_a)^3 + c_a \dot{\alpha}_a = 0, \end{cases} \tag{12}$$

with $\alpha_a = \theta_a - \theta_l$.

### 4.2. Determination of the NES parameters: a parametric study

The values of the NES parameters, namely the nonlinear stiffness $k_{\theta_{nl}}$, the moment of inertia $J_{\text{add}}$, and the damping coefficient $c_a$, have to be selected carefully. A parametric study is performed to determine these values. The objective is not to find the best set of values for the NES, but rather to understand whether the introduction of the NES can enlarge the range of working input voltages for which stick-slip limit cycling is avoided. Therefore, an initial set of values is used and adapted to obtain the largest range of input voltages leading to stable equilibrium solutions and the avoidance of stick-slip limit cycling (i.e., periodic solutions).

For obvious practical reasons, the adopted mass ratio between the NES and the drill-string system should be as small as possible. Moreover, so far, as no methodology exists for the NES design, we chose the same design rules as those considered in previous studies. The NES inertia is initially set to 5% of the total inertia of the system. In practice, this value may seem to be large, however, the focus of the study is on the new dynamics created by the introduction of an NES in a nonlinear (discontinuous) primary structure. As the inertia of the

Table 4
Modification of the nonlinear stiffness $k_{\theta_{nl}}$

| $k_{\theta_{nl}}$ | | Stable equilibria | Other solutions | |
|---|---|---|---|---|
| N m/rad$^3$ | $n \times k_{\theta_{nl_{\text{init}}}}$ | Range | Range | Type |
| 0.0025 | 1 | [1.7 → [ V | [0.3 → 1.7 [ V | Periodic solutions |
| 1 | $4 \times 10^2$ | [3.5 → [ V | [0.3 → 3.5 [ V | Periodic solutions |
| $1 \times 10^{-2}$ | 4 | [2.9 → [ V | [0.3 → 2.9 [ V | Periodic solutions |
| $1 \times 10^{-3}$ | $4 \times 10^{-1}$ | [2.1 → [ V | [0.3 → 2.1 [ V | Periodic solutions |
| $1 \times 10^{-7}$ | $4 \times 10^{-5}$ | [2.6 → [ V | [0.3 → 2.6 [ V | Periodic solutions |

Table 5
Modification of the moment of inertia $J_{\text{add}}$

| $J_{\text{add}}$ | | Stable equilibria | Other solutions | |
|---|---|---|---|---|
| kg m$^2$ | % of $J_{\text{tot}}$ | Range | Range | Type |
| 0.25895 | 50 | [2.5 → [ V | [0.3 → 2.5 [ V | Periodic solutions |
| 0.05179 | 10 | [2.1 → [ V | [0.3 → 2.1 [ V | Periodic solutions |
| 0.03107 | 6 | [1.9 → [ V | [0.3 → 1.9 [ V | Periodic solutions |
| 0.02072 | 4 | [1.6 → [ V | [0.3 → 1.6 [ V | Periodic solutions |
| 0.01294 | 2.5 | [2.8 → [ V | [0.3 → 2.8 [ V | Periodic solutions |
| 0.00259 | 0.5 | [3.6 → [ V | [0.3 → 3.6 [ V | Periodic solutions |

Table 6
Modification of the damping coefficient $c_a$

| $c_a$ | | Stable equilibria | Other solutions | |
|---|---|---|---|---|
| N m s/rad | $n \times c_{a_{\text{init}}}$ | Range | Range | Type |
| 0.1050 | 10 | [2.8 → [ V | [0.3 → 2.8 [ V | Periodic solutions |
| 0.0210 | 2 | [1.7 → [ V | [0.3 → 1.7 [ V | Periodic solutions |
| 0.00525 | 0.5 | [2.1 → [ V | [0.3 → 2.1 [ V | Periodic solutions |
| 0.00105 | 0.1 | [3.5 → [ V | [0.3 → 3.5 [ V | Periodic solutions |

Table 7
Selected NES parameters $k_{\theta_{nl}}$

| Set no. | $k_{nl}$ (N m/rad$^3$) | $J_{\text{add}}$ (kg m$^2$) | $c_a$ (N m s/rad) |
|---|---|---|---|
| 1 | 0.002515 | 0.025895 | 0.0105 |
| 2 | 0.002515 | 0.020716 | 0.0105 |
| 3 | 0.002515 | 0.025895 | 0.0210 |

additional disc is close to the one of the lower disc, the NES dashpot will be chosen such that its viscous damping coefficient has a value close to that of the lower disc $b_l$. Finally, the determination of the nonlinear (cubic) stiffness is based on the linear stiffness of the string of the primary system. The aim is to find a value of the nonlinear stiffness that creates an elastic torque of the same order of magnitude than that characterizing the primary system. The initial set of parameters is given in Table 3.

Several simulations were carried out by modifying a single parameter in the initial set in order to assess the impact of the modification on the dynamical behavior; such impact being revealed through bifurcation

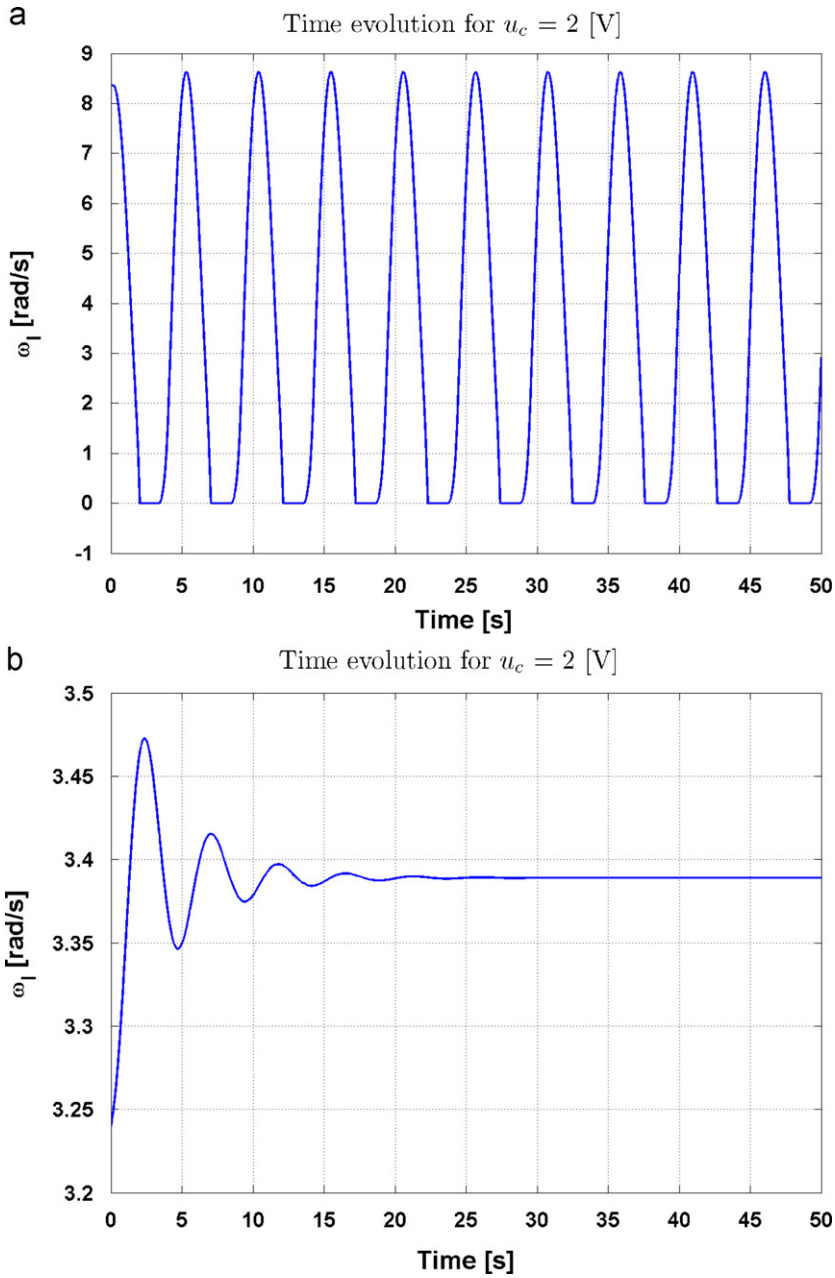


Fig. 11. Time evolution for a given input voltage at DC-motor $u_c = 2$ V: (a) primary system without NES; and (b) primary system with NES with parameter set 1.

diagrams. All the results related to these numerical experiments are available in Ref. [17] and are summarized in Tables 4–6 for the modification of the nonlinear stiffness $k_{\theta_{nl}}$, moment of inertia $J_{\text{add}}$ and viscous coefficient $c_a$, respectively. Depending on the parameter values, the existence of periodic solutions is restricted to wider or narrower input voltage ranges. For instance, the selection of the nonlinear spring coefficient is crucial, as shown in Table 4. For some values, the periodic solutions exist until 3.5 V, whereas for others values they exist only until 1.7 V. The parametric study in [17] showed that the sets of parameters in Table 7 give interesting results in terms of LCO suppression.

For illustration, Fig. 11 clearly shows that the presence of the NES stabilizes the drill-string system for an input voltage of 2 V. It's worth being mentioned that the equilibrium of the system without NES: $\omega_l = \omega_u = \omega_{eq}$ and $\alpha = \alpha_{eq}$ exists in the system with NES in the sense that $\omega_l = \omega_u = \omega_a = \omega_{eq}$ and $\alpha = \alpha_{eq}$. We note that the new equilibrium solution provided by the NES might not be the only steady-state solution for this particular voltage. This is discussed in the next section.

## 5. Detailed analysis of a drill-string system with an NES

This section carries out a detailed analysis of the nonlinear dynamics of a drill-string system coupled to an NES. The main results consist of bifurcation diagrams for the three sets of NES parameters in Table 7. Moreover, the basins of attraction of the solutions (for given input voltages) are presented. The purpose is to investigate the NES efficacy and robustness together with the complexity of the resulting dynamical behavior. Finally, the wavelet transform is applied to the time series in order to demonstrate possible resonance captures between the drill-string system and the NES.

### *5.1. NES efficacy*

To examine the NES efficacy, the comparison of bifurcation diagrams with and without the absorber is performed. Fig. 12(a)–(e) clearly show the improvement in the dynamical behavior brought by the NES, for all parameter sets considered:

- The range of input voltages leading to stable equilibria (i.e., nominal behavior of the drill-string system) is increased.
- The LCOs of the drill-string system can be completely eliminated, at least in certain voltage ranges.
- The NES can also achieve partial LCO suppression; i.e., it can reduce the amplitude of the surviving limit cycles in the regions where complete elimination is not possible (mainly below 1.8 V).

The comparison of the bifurcation diagrams in Fig. 12(b) and (e) highlights that, depending on the NES parameters, the dynamics in the partial suppression region can be relatively simple (set #3) or much more complex (set #1).

For a quantitative assessment of the NES efficacy, three different criteria are considered:

1. The percentile reduction of the range of voltages leading to unstable equilibria and their transformation into locally asymptotically stable equilibria.
2. The percentage of voltages leading to (locally or globally) stable equilibria over the range $[0, 3.83]$ V.
3. The percentage of the input voltage range $[1.69, 3.83]$ V for which locally stable equilibrium solutions are transformed into globally stable equilibrium solutions (or equivalently the complete LCO suppression by the NES).

The numerical values related to these criteria are listed in Table 8 and show that the third parameter set creates a wider range of voltages leading to equilibrium solutions only. Only sets #1 and #3 are considered in this table as their respective bifurcation diagram present clear differences due to the difference of damping coefficient. Another advantage of this parameter set is that it leads to a smoother bifurcation diagram (i.e. to more predictable steady-state behavior).

A complete characterization of the different bifurcation diagrams is beyond the scope of this paper. However, we note that transitions between the different branches may be realized through discontinuous fold bifurcation and subcritical Hopf bifurcation points.

One objective of passive vibration mitigation is to perturb the primary system to the lowest extent. Accordingly, the NES should be as light as possible. The second parameter set is characterized by a rotating inertia for the NES equal to 4% of the total rotating inertia (instead of 5% for sets #1 and #3). Fig. 12(d) compares the bifurcation diagrams for sets #1 and #2. Even if the global shape of the diagrams is the same,

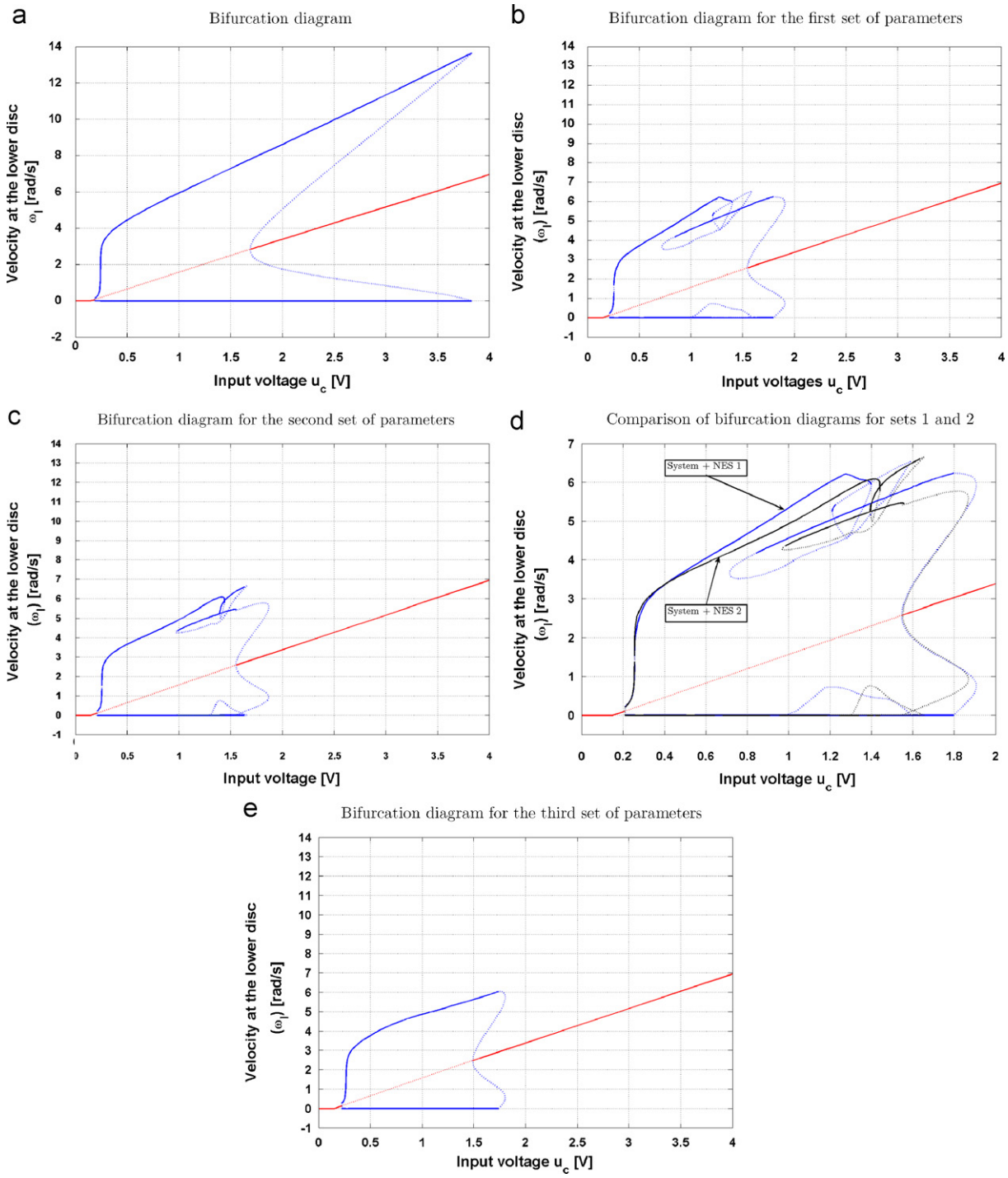


Fig. 12. Illustration of bifurcation diagrams: (a) primary system; (b) system + NES 1; (c) system + NES 2; (d) comparison between NES 1 and 2; and (e) system + NES 3.

a small difference in the rotating inertia creates important modifications in the dynamical behavior. This confirms the complexity of the new dynamics created, due to the strongly nonlinear characteristic of the NES.

Table 8
Stabilization of the drill-string system (quantitative assessment)

| Criterion | First set (%) | Third set (%) | Difference (%) |
|---|---|---|---|
| 1 | 11.04 | 15.89 | 4.85 |
| 2 | 65.04 | 66.95 | 1.91 |
| 3 | 94.95 | 97.66 | 2.71 |

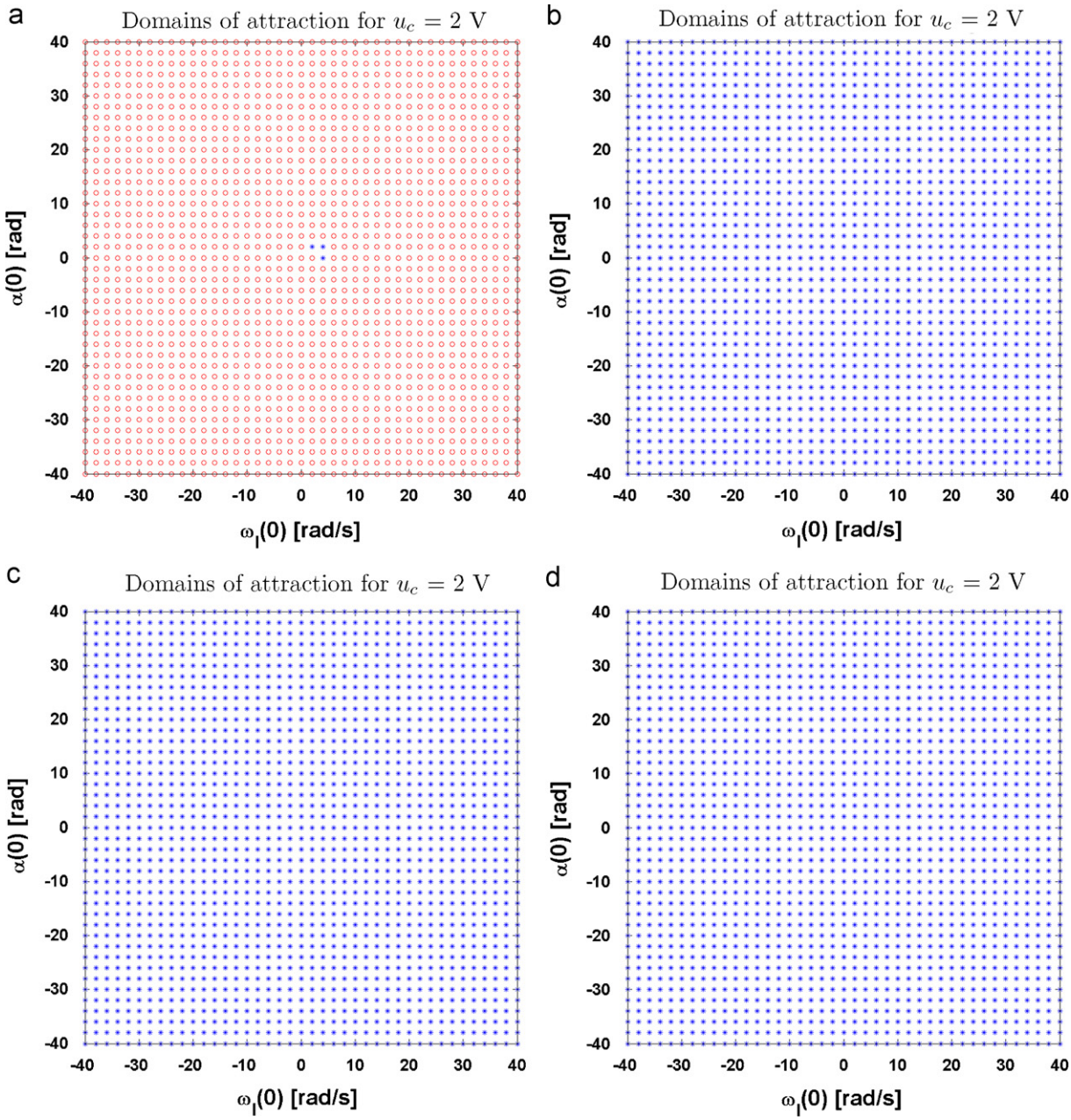


Fig. 13. Domains of attraction for an input voltage $u_c = 2$ V; red circles = periodic solutions, blue stars = equilibrium points: (a) primary system; (b) system + NES 1; (c) system + NES 2; and (d) system + NES 3.

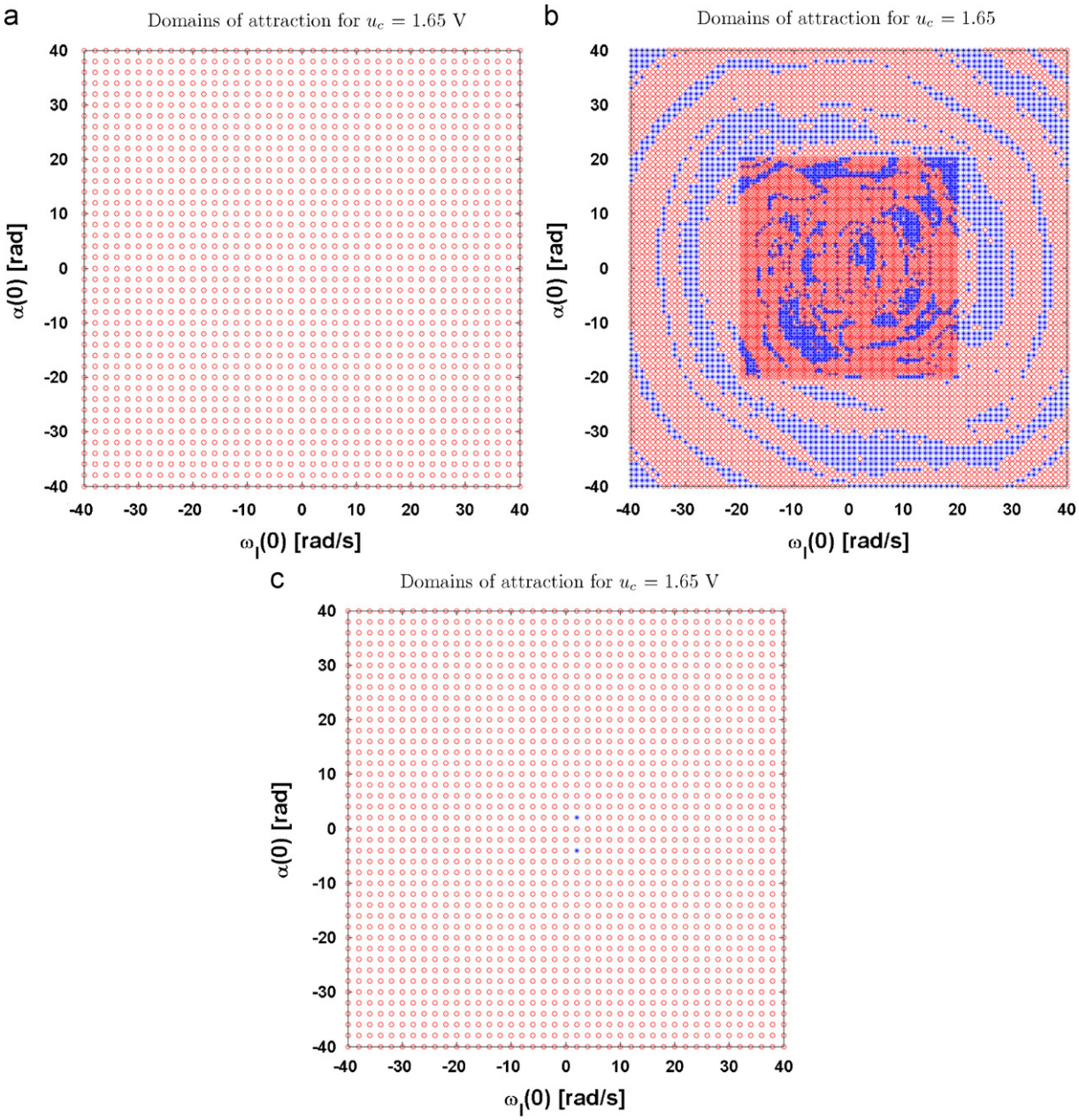


Fig. 14. Domains of attraction for an input voltage $u_c = 1.65$ V; red circles = periodic solutions, blue stars = equilibrium points: (a) primary system; (b) system + NES 1; and (c) system + NES 3.

## 5.2. Robustness of LCO suppression

One key feature of nonlinear systems is that several (quasi-)periodic solutions and/or equilibrium points as well as chaotic solution may coexist over certain frequency ranges. For instance, a stable LCO may coexist with a stable equilibrium point at a certain input voltage. Depending on the initial conditions, the convergence toward either solution can be achieved. To study the robustness of the passive control realized with the NES, it is therefore meaningful to study the basins of attraction of each kind of steady-state solutions (i.e., equilibria and periodic solutions).

The system composed of the drill-string and the NES is characterized by five state-space variables, meaning that the basins of attraction lie in a five-dimensional space. For graphical representation, only two state-space variables are considered, namely the velocity of the lower disc $\omega_l$ and the deformation of the string of the primary system $\alpha$. All other state variables are set to zero at the initial time.

Figs. 13 and 14 enable us to obtain improved insight into the change of the basins of attraction when an NES is added to the drill-string system for voltages of 2 and 1.65 V, respectively. Red circles and blue stars refer to the initial conditions leading to stable LCOs and equilibria, respectively. It can be observed that:

(1) For an input voltage of 2 V (Fig. 13), the transformation of locally stable equilibrium points into globally stable equilibrium points is evident for the three parameter sets considered in this study.
(2) For an input voltage of 1.65 V (Fig. 14) and unlike the third parameter set, we note the complicated dynamics introduced by the NES for the first parameter set. These diagrams also confirm that the LCOs

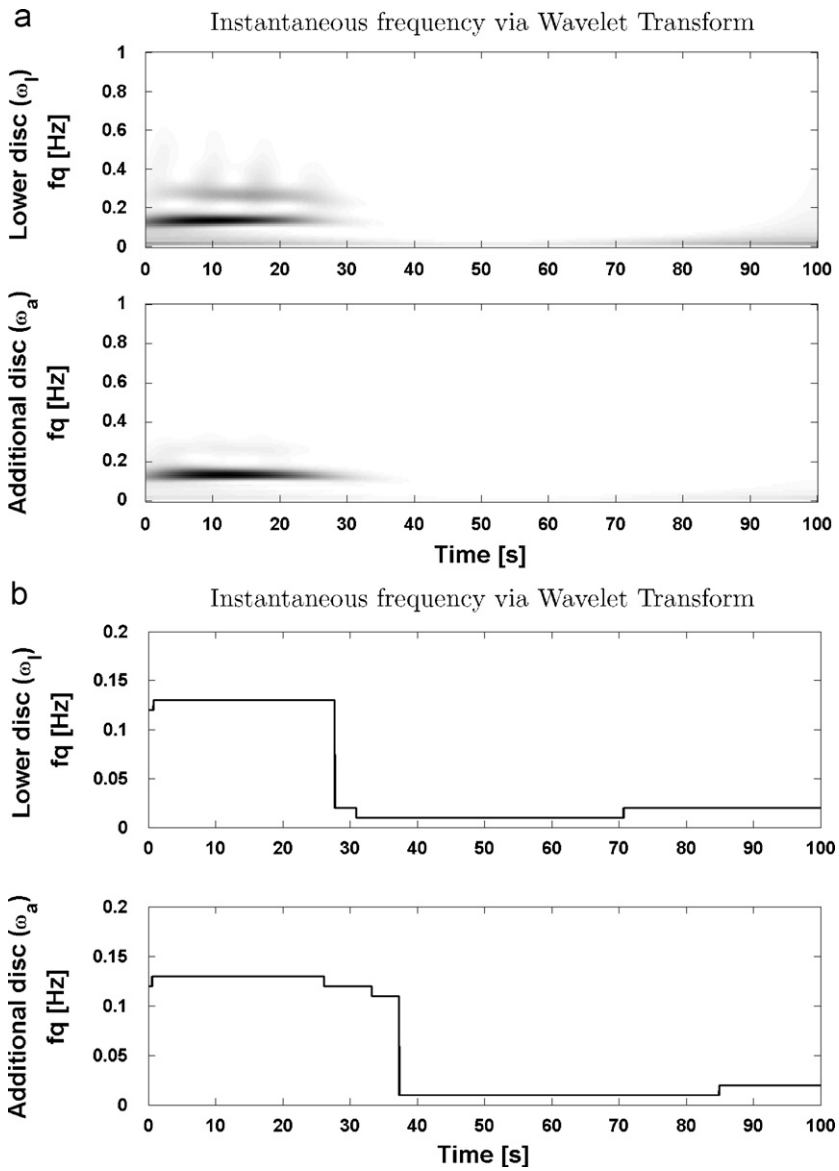


Fig. 15. Instantaneous frequency via wavelet transform ($u_c = 2$ V; parameter set #1): (a) shaded representation; and (b) maximum frequencies.

originally present in the drill-string system have been transformed into locally asymptotically stable equilibrium points.

Finally, these observations confirm that the equilibrium branch $e_4$ (using the same definition as for Fig. 8) of the bifurcation diagrams in Fig. 12(b) and (e) consists of locally and globally asymptotically stable equilibrium points.

### 5.3. Identification of resonance captures

The purpose of this section is to apply the wavelet transform [24] to the time series of the responses of the drill-string system in order to study possible resonance captures between the drill-string system and the NES. The wavelet transform (WT) is a suitable technique to analyze the temporal evolution of the dominant

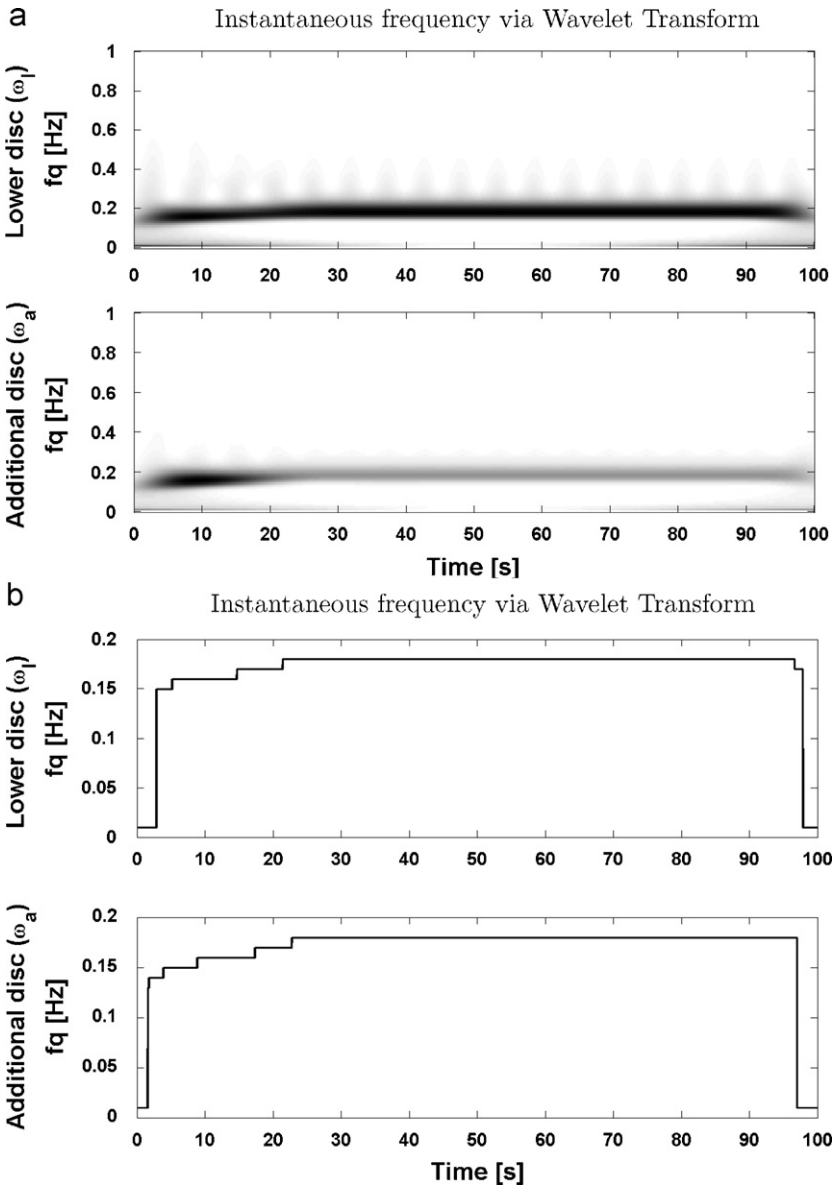


Fig. 16. Instantaneous frequency via wavelet transform ($u_c = 1.5$ V; parameter set #2): (a) shaded representation; and (b) maximum frequencies.

frequency components of nonlinear signals. The comparison of the instantaneous frequency of the velocity at the lower disc and at the NES provides a robust means of verifying the occurrence of resonance captures, or frequency locking during the transient dynamics.

Figs. 15 and 16 depict the instantaneous frequencies of the velocity at the lower ($\omega_l$) disc and at the NES ($\omega_a$) for voltages leading to an equilibrium point (2 V) and a periodic solution (1.5 V), respectively. These figures seem to confirm the resonance capture and the locking in the transient phase. In fact, the NES, which has no preferential resonant frequency, tunes itself to the frequency of the developing instability. This resonance phenomenon leads to targeted energy transfers from the drill-string system to the NES. The energy is confined in the absorber, where it is eventually dissipated by the dashpot.

## 6. Concluding remarks

Self-sustained vibrations may appear in mechanical systems for various reasons and often limit the performance of such systems or even cause damage or system failure. In this study, the focus is on friction-induced vibrations in drill-string systems. As a benchmark we considered a rotor-dynamic system with (set-valued) friction and flexibilities.

This paper investigated the possibility of passively mitigating these friction-induced vibrations using a nonlinear absorber characterized by an essential stiffness nonlinearity. The motivation for using a NES is its absence of preferential resonance frequency, which enables it to resonate with and extract energy from the drill-string system in an a priori frequency-independent fashion.

The parametric study demonstrated that the NES can completely eliminate the instabilities in a relatively wide range of parameter (for which the system without NES exhibits limit cycling). In addition, the NES can also achieve partial limit cycling suppression; i.e., it reduces the 'amplitude' of the remaining limit cycles in the regions where complete elimination is not possible. The addition of an NES to a drill-string system clearly improves the global dynamical behavior of the system and substantially extends its domain of operation.

Because a complete limit cycle suppression in the whole range parameters considered was not possible, future research should perform a more exhaustive search of the design space. In this context, optimization methods should help to obtain broader suppression results. The comparison of the present results with the performance achieved with active control would also be an interesting contribution.

## Acknowledgments

The authors R. Viguié and G. Kerschen would like to acknowledge the Belgian National Fund for Scientific Research (FRIA & FNRS fellowships) for its financial support.

## References

[1] A.F. Vakakis, O.V. Gendelman, Energy pumping in nonlinear mechanical oscillators: part II—resonance capture, ASME Journal of Applied Mechanics 68 (2001) 42–48.
[2] Y.S. Lee, G. Kerschen, A.F. Vakakis, P. Panagopoulos, L.A. Bergman, D.M. McFarland, Complicated dynamics of a linear oscillator with an essentially nonlinear local attachment, Physica D 204 (2005) 41–69.
[3] G. Kerschen, Y.S. Lee, A.F. Vakakis, D.M. McFarland, L.A. Bergman, Irreversible passive energy transfer in coupled oscillators with essential nonlinearity, SIAM Journal on Applied Mathematics 66 (2006) 648–679.
[4] Y.S. Lee, A.F. Vakakis, L.A. Bergman, D.M. McFarland, Suppression of limit cycle oscillations in the van der Pol oscillator by means of passive non-linear energy sinks, Structural Control & Health Monitoring 13 (2006) 41–75.
[5] Y.S. Lee, A.F. Vakakis, L.A. Bergman, D.M. McFarland, G. Kerschen, Suppression of aeroelastic instability by means of broadband passive targeted energy transfers: part I, theory, AIAA Journal 45 (2007) 693–711.
[6] N. Mihajlovic, Torsional and Lateral Vibrations in Flexible Rotor Systems with Friction, Technische Universiteit Eindhoven, 2005.
[7] N. Mihajlovic, N. van de Wouw, R.C.J.N. Rosille, H. Nijmeijer, Interaction between torsional and lateral vibrations in flexible rotor systems with discontinuous friction, Nonlinear Dynamics (2007), accepted for publication.
[8] R.A. Cunningham, Analysis of downhole measurements of drill string forces and motions, ASME Journal of Engineering for Industry 90 (1968) 208–216.
[9] J.D. Jansen, L. van den Steen, Active damping of self-excited torsional vibrations in oil well drill-string, Journal of Sound and Vibration 179 (4) (1995) 647–668.

[10] R.I. Leine, D.H. van Campen, W.J.G. Keultjes, Stick-slip whirl interaction in drill-string dynamics, ASME Journal of Vibration and Acoustics 124 (2002) 209–220.
[11] L. Van den Steen, Suppressing stick-slip-induced drill-string oscillations: a hyper stability approach, Ph.D. Thesis, University of Twente, 1997.
[12] J.F. Brett, Genesis of torsional drill-string vibrations, SPE Drilling Engineering 7 (3) (1992) 168–174.
[13] E. Kruzer, O. Kust, Analyse selbsterregter drehschwingugnen in torsionsstben, ZAMM—Journal of Applied Mathematics and Mechanics/Zeitschrijft fuer Angewandte Mathematik und Mechanik 76 (10) (1996) 547–557.
[14] T. Richard, C. Germay, E. Detournay, Self-excited stick-slip oscillations of drill bits, Comptes Rendus Mecanique, French Academy of Sciences 332 (2004) 619–626.
[15] C. Germay, N. van de Wouw, H. Nijmeijer, R. Sepulchre, Nonlinear drillstring dynamics analysis, SIAM Journal on Applied Dynamical Systems (2007), accepted for publication.
[16] N. Mihajlovic, N. van de Wouw, M.P.M. Hendriks, K. Nijmeijer, Friction-induced limit cycling in flexible rotor systems and experimental drill-string set-up, Nonlinear Dynamics, accepted for publication (Special issue on experimental analysis and control of non-smooth dynamical systems, Theory and Experiments 6(3) (2006) 273–291).
[17] R. Viguié, Passive vibration mitigation in rotor systems using nonlinear energy sinks, M.S. Thesis, University of Liège, 2006.
[18] B. Armstrong-Hélouvry, Control of Machines with Friction, Kluwer Academic Publisher, Boston, 1991.
[19] C. Canudas de Wit, H. Olsson, K.J. Astrm, P. Lischinsky, A new model for control of systems with friction, IEEE Transaction on Automatic Control 40 (3) (1995) 419–425.
[20] R.H.A. Hensen, controlled mechanical systems with friction, Ph.D. Thesis, Eindhoven University of Technology, The Netherlands, 2002.
[21] H. Olsson, Control systems with friction, Ph.D. Thesis, Lund Institute of Technology, Sweden, 1996.
[22] R.I. Leine, K. Nijmeijer, Dynamics and Bifurcations of Non-smooth Mechanical Systems, Springer, Berlin, 2004.
[23] H.B. Keller, Numerical Solution of Two-Point Boundary Value Problems, Society of Industrial and Applied Mathematics, Philadelphia, 1976.
[24] S. Mallat, A Wavelet Tour of Signal Processing, second ed., Academic Press, New York, 1999.